Layer-Dependent Ultrafast Carrier and Coherent Phonon Dynamics in Black Phosphorus

Xianchong Miao,[†,‡] Guowei Zhang,[†,‡] Fanjie Wang,[†,‡] Hugen Yan,*[,†,‡] and Minbiao Ji*[,†,‡]

[†]State Key Laboratory of Surface Physics and Department of Physics, Key Laboratory of Micro and Nano Photonic Structures (Ministry of Education), Fudan University, Shanghai 200433, China

[‡]Collaborative Innovation Center of Advanced Microstructures, Nanjing 210093, China

S Supporting Information

ABSTRACT: Black phosphorus is a layered semiconducting material, demonstrating strong layer-dependent optical and electronic properties. Probing the photophysical properties on ultrafast time scales is of central importance in understanding many-body interactions and nonequilibrium quasiparticle dynamics. Here, we applied temporally, spectrally, and spatially resolved pump−probe microscopy to study the transient optical responses of mechanically exfoliated few-layer black phosphorus, with layer numbers ranging from 2 to 9. We have observed layer-dependent resonant transient absorption spectra with both photobleaching and red-shifted photoinduced absorption features, which could be attributed to band gap renormalization of higher subband transitions. Surprisingly, coherent phonon oscillations with unprecedented intensities were observed when the probe photons were in resonance with the optical transitions, which correspond to the low-frequency layer-breathing mode. Our results reveal strong Coulomb interactions and electron−phonon couplings in photoexcited black phosphorus, providing important insights into the ultrafast optical, nanomechanical, and optoelectronic properties of this novel two-dimensional material.

KEYWORDS: Black phosphorus, carrier dynamics, coherent phonon, pump−probe microscopy, ultrafast spectroscopy
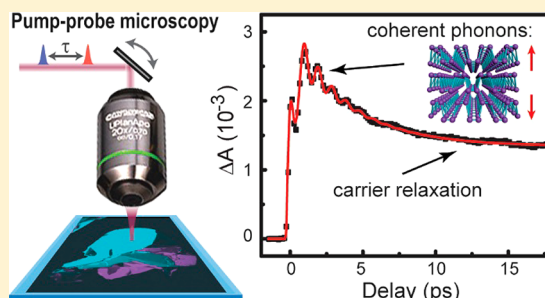
As a newly emerged member in the two-dimensional (2D) materials family, black phosphorus (BP) has demonstrated extraordinary properties including high carrier mobility,[1] anisotropy,[2,3] and layer-dependent direct band gap covering a wide spectral range from visible to mid-infrared (0.3−2 eV).[4−6] As a result, BP has become a promising candidate for use in high-speed electronic devices and in low noise mid-infrared optoelectronic devices. Moreover, because of its puckered honeycomb lattice symmetry with armchair (AC) and zigzag (ZZ) orientations, BP has exhibited distinct anisotropic in-plane properties, such as carrier mobility,[3,7] mechanical flexibility,[8] thermal conductivity,[9,10] and optical responses,[5,6] providing opportunities for novel polarization-sensitive devices. Exploiting these unique properties, BP-based solar cells,[11] photodetectors,[12] and transistors[13] have been demonstrated, showing their commercial viability for future applications.

Various optical techniques have been extensively applied to study the electronic and vibrational properties of BP. Linear and steady-state optical measurements of few-layer BP have shown anisotropic and layer-dependent Raman scattering,[14,15] infrared (IR) and visible absorption,[5,6] and photoluminescence (PL).[16] Layer-dependent third-order nonlinear optical susceptibilities of few-layer BP have also been characterized via third harmonic generation (THG).[17,18] Although the ultrafast carrier dynamics of bulk and thin film BP (thickness larger than 20 nm) have recently been studied, indicating enhanced anisotropy of hot carriers and dynamical conductivity,[19−21]

the layer dependence of ultrafast optical response of few-layer BP remains uncovered. This layer-dependent behavior could provide crucial information regarding the many-body interactions and electron−phonon couplings in low-dimensional materials, as shown in transition-metal dichalcogenides (TMDCs) and single-walled carbon nanotubes (SWNTs).[22−25]

Here, we report the first comprehensive ultrafast optical investigation of the photoexcited carriers and coherent phonon dynamics in few-layer BP with layer numbers ranging from 2 to 9. We have discovered the resonance features of the transient absorption spectra, echoing with the layer-dependent linear absorption peaks of the excitons. A significant band gap renormalization effect could be clearly seen in the transient spectra, which reflects the strong electron−electron interactions in few-layer BP. Such an effect has been found to be vitally important in the band structures and excitonic effects in TMDCs, in both ground and photoexcited states.[23,25,26] Furthermore, strongly enhanced coherent phonon dynamics show up only when the probe energies are in resonance with the transient absorption, indicating giant electron−phonon couplings in the photoexcited few-layer BP. The layer dependence of the phonon frequencies could be explained with linear chain model of the layer-breathing mode. These rich

ultrafast spectroscopic features of few-layer BP promise great research opportunities in studying the photophysics of this novel material, and its potential applications in fast photonics and optoelectronics.

Results and Discussion. *Temporally and Spectrally Resolved Pump—Probe Microscopy.* The setup of our home-built laser-scanning pump—probe microscopy with high temporal and spatial resolutions is described in Materials and Methods and Figure S1. Using this system, we could detect the transient absorption (TA) signal with shot-noise limited sensitivity at imaging high speed (less than 1 s/frame). Differential absorbance ($\Delta A = -\Delta T/T$) was measured in the transmission mode, with fixed pump photon energy of 1.2 eV and tunable probe energy between 1.25 and 1.65 eV. Both laser beams were polarized in the AC direction to obtain maximum TA intensities, except for the anisotropy measurements. Time delays (τ) between pump and probe pulses were synchronized with the image frames to acquire time-resolved TA images, achieving rich spatial—temporal information on the samples. In addition, sequentially tuning the probe wavelengths allows us to collect the spectral information on the ultrafast transient dynamics. Such a pump—probe microscopy not only provides a high-throughput means to simultaneously measure the spatially heterogeneous ultrafast dynamics within a sample but also efficiently reduces optical damage via rapid scanning of focused laser spots (Figure S2), which is crucial in studying vulnerable few-layer BP.

Few-layer BP samples were prepared by mechanical exfoliation as described previously.[1] Freshly exfoliated BP flakes on transparent polydimethylsiloxane (PDMS) substrates were used directly for optical measurements. Fingerprint IR absorption spectra were taken to determine the layer thicknesses prior to ultrafast pump—probe measurements.[6] Typical IR measurements would require relatively large-area BP samples ($>20 \times 20$ μm^2) because of the large diffraction limited laser spots using long wavelengths. However, for samples with small sizes of interest, as shown in the bright-field image (Figure 1A), where adjacent small-area 3- and 4-layer BPs coexist, the IR spectrum shows only a mixture of characteristic spectra from both layers (Figure 1B). While optical contrast may provide insightful layer information in this situation, we demonstrate that pump—probe microscopy could serve as an alternative method to determine layer numbers based on layer-dependent transient optical responses, without resorting to large size samples.

Skimming through the time-resolved pump—probe images under a fixed probe photon energy (1.55 eV), we could readily see that different regions of the sample demonstrate significantly different transient behaviors (Movie S1). This observation could also be clearly visualized in the TA images taken at different time delays, where the contrasts between 3L, 4L, 7L, and thick BP regions change remarkably when τ is varied from 0.3 to 3.5 ps (Figure 1C—E). Area-averaged TA traces of the above four regions demonstrate distinctively different transient dynamics (Figure 1F). For the thick and 4L BP regions, TA dynamics show an initial photobleaching (PB) as indicated by the negative ΔA, followed by a rapid recovery and growth of positive photoinduced absorption (PA). Longer delay time measurements indicate a slow ($\sim$90 ps) relaxation for the PA component (Figure S3). The overall transient behavior of the 4L and thick regions is similar to that of the bulk and thin film BP.[20] In contrast, 3L and 7L BP shows very different transient dynamics, with little PB contribution but
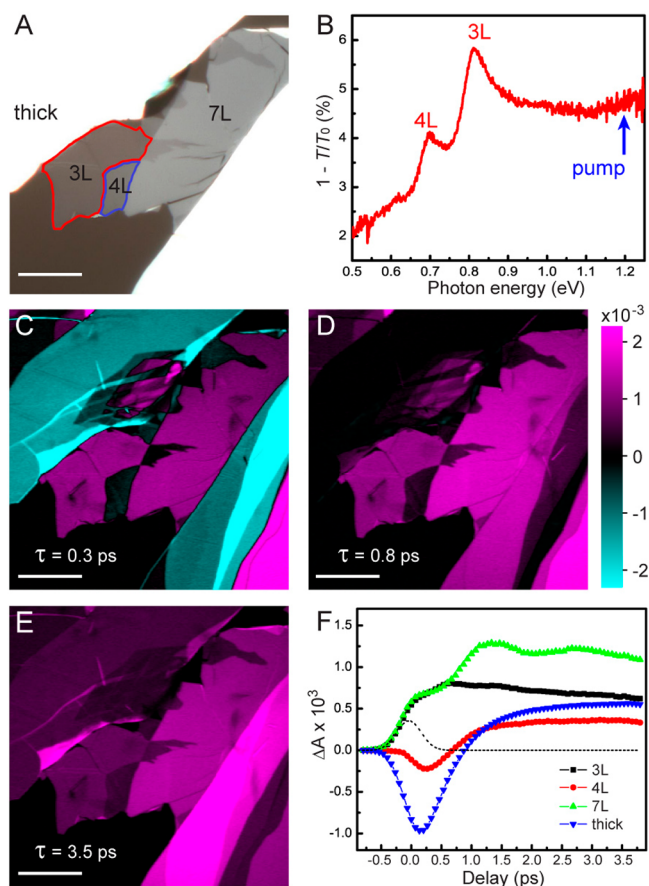
Figure 1. Few-layer BP samples and pump—probe microscopy. (A) Optical image of a BP sample with heterogeneous thicknesses. (B) Infrared spectrum of the 3L and 4L region. Blue arrow indicates the pump energy of 1.2 eV. The tunable probe energy ranges from 1.25 to 1.65 eV. (C—E) TA images taken at different time delays between pump and probe pulses with a probe energy of 1.52 eV. The color bar shows the intensity and sign of the TA signal. (F) TA traces from regions of different thicknesses. The dashed curve represents the cross-correlation between pump and probe. Scale bar: 20 μm.

oscillating PA signals. These oscillations are attributed to coherent phonons (CP) generated by impulsive excitation, and quantitative studies of layer-dependent CP properties are presented later in the Letter. Despite these time-domain differences, it is difficult to precisely correlate the layer numbers to the transient responses measured at a single probe energy, and a spectral dimension must be added.

Varying probe photon energies results in dramatic changes of the transient responses of few-layer BP, as seen in the large contrast differences between TA images probed at 1.55, 1.46, and 1.38 eV under a fixed time delay of 0.3 ps (Figure S4). The thick parts of the BP flakes exhibit constant negative ΔA, whereas the 4L region experiences a transition from PB to PA with a decreasing probe energy. In addition, the TA traces at these probe energies show the emergence of strong oscillations in the PA dominated curves, whereas they are absent in the PB dominated ones (Figure S4F). Because of the large spectral variations, complete characterization of layer-dependent transient dynamics must require spectrally and temporally resolved TA measurements. These results (2—9 layers and bulk BP) are plotted as individual 2D spectrum, demonstrating unique characters of each layered BP (Figure S5).
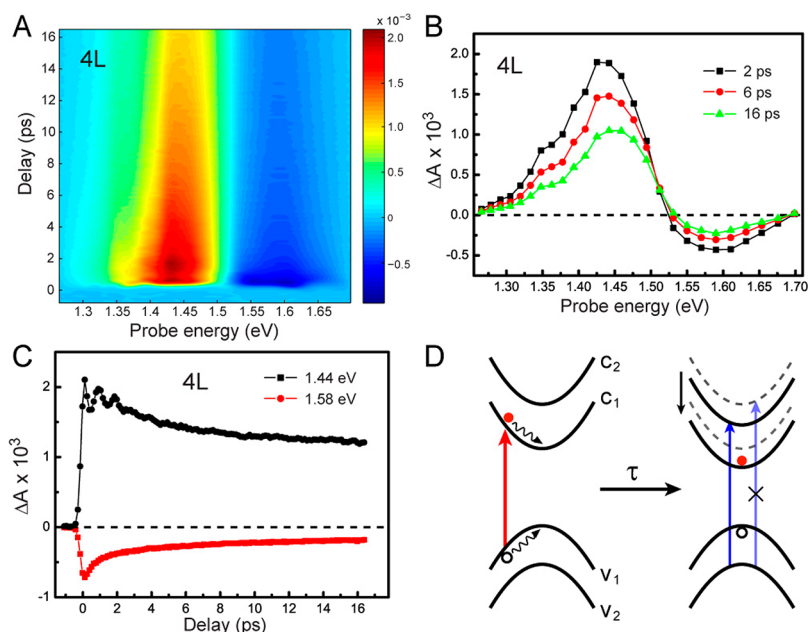
Figure 2. Transient optical response of 4L BP. (A) Temporally and spectrally resolved TA signal of 4L BP. (B) TA spectra taken at different time delays. The dashed line represents zero signal. (C) Time-resolved TA traces probed around the peak and valley. (D) Schematic illustration of the band gap renormalization effect that shrinks the electronic band gaps. The red arrow represents pump excitation, and the blue arrows represent optical probing near E_{22} transition. The cross mark indicates the absorption reduction of the original E_{22} transition.
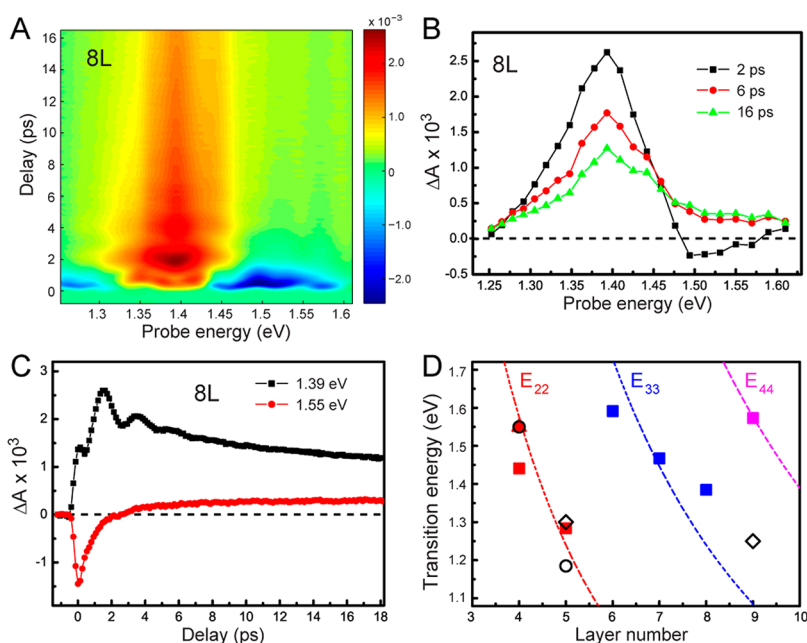
Figure 3. Transient dynamics of 8L BP and layer-dependent resonances. (A) Temporally and spectrally resolved TA signal of 8L BP. (B) TA spectra taken at different time delays. The dashed line represents zero signal. (C) TA traces probed around the peak and valley showing different dynamical features. (D) Layer-dependent resonant energies of our PA (colored squares) and PB (red triangle) bands, in comparison with IR/visible absorption results (circles from ref 5 and diamonds from ref 6) and calculated excitonic transition energies (dashed curves).

Resonant Transient Absorption and Band Gap Renormalization. Resonance features of the TA spectra are readily seen with layer-dependent peak positions in most of the few-layer samples, whereas they do not exist in thick/bulk BP samples. For a detailed demonstration and analysis, here we mainly focus on the results of 4L (Figure 2) and 8L (Figure 3) BP samples. A typical 2D plot of the TA spectra of 4L BP exhibit clear resonant bands within our detection window: a negative PB band around 1.55 eV and a positive PA band around 1.44 eV

(Figure 2A). Transient spectra at various time delays show similar differential line shapes (Figure 2B). Also, the TA traces probed at the peak and valley appear to have similar overall dynamics with opposite signs (Figure 2C). Given that the PB peak matches very well with the E_{22} exciton in 4L BP[5,6] and that the PA band is red-shifted compared with the PB band, we assign the spectral features to be dominated by band gap renormalization (BGR) due to the strong interactions between the excited-state carriers that shrink the electronic gaps. As
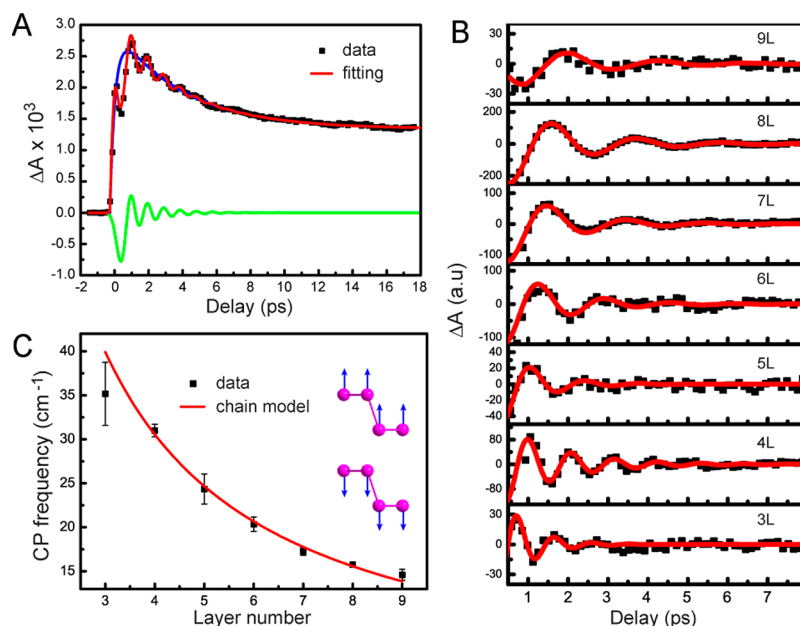
Figure 4. Layer-dependent coherent phonon dynamics. (A) A typical TA trace of 4L BP probed at 1.46 eV, fitted with the sum of carrier dynamics (blue), coherent phonon dynamics (green), and instrument response at time zero (not shown). (B) Layer-dependent CP components with the fitting results. (C) Layer-dependent CP frequency fitted with the linear chain model and illustration of the layer-breathing mode.

schematically depicted in Figure 2d, the reduced E_{22} transition energy results in the absorption reduction (PB) of the original optical transition with simultaneous increased absorption (PA) from the red-shifted E_{22} band. Our results also indicate the enhanced optical strength of the renormalized E_{22} transition. Although the overall dynamics of PB and PA appear to be similar due to their common origin (recombination of photocarriers), we could clearly visualize a major difference between them: remarkable coherent phonon oscillations exist in resonance with the PA band, while they are negligible in the PB transients (Figure 2C). The absence of CP in the PB band supports the BGR hypothesis since PB mainly reflects ground state depletion (due to band shift) and hence is insensitive to excited-state lattice vibrations.

Ideally, we should probe a much wider spectral range covering more exciton peaks. However, it would require an optical system with supercontinuum generation and detection from mid-IR to visible, which is extremely demanding. We partially compromise our spectral limitation by probing different exciton transitions with varying layer numbers, within the same spectral window. For 8L BP, the E_{33} exciton may have fallen into our detection window and its transient spectra could be obtained (Figure 3), with similar yet different transient behaviors from those of 4L specimens. The observation of a strong PA band (1.39 eV) along with enhanced CP oscillations replicates the results of 4L BP. However, in contrast to the similar dynamics of PA and PB bands observed in 4L BP, the PB band occurs to be much shorter lived than PA in 8L samples. As the time delay varies, the PB feature rapidly vanishes (Figure 3B), and the early time dynamics probed at the peak and valley both show a growing PA component of ~0.9 ps (Figure 3C). These results indicate that multiple effects have contributed to the transient dynamics in 8L BP. Linear absorption spectra inform that more continuum states could be excited at higher excitation energies, as is also the case for thicker BP under the same excitation energy. Therefore, in addition to the BGR effect of excitonic transitions with narrow

resonances, excited free-carriers in thicker BP contribute to the broad featureless PA dynamics similar to the bulk response.[21,27] The early growing PA may originate from the band-filling effect when the initial hot carriers relax and thermalize, followed by the slow relaxation of photocarriers (Figure S6).

The resonant TA phenomena could not be explained by free-carrier absorption using the Drude model as assigned in previous measurements in bulk/thin film BP.[27] Similar PB and PA resonances have been observed in SWNTs,[28] with PB bands corresponding to the Pauli blocking of S_{11} and S_{22} excitons and PA bands assigned to excited-state absorption (ESA) of intersubband transitions. However, the cause of PA resonances in few-layer BP must exclude ESA because of two major reasons: (1) intersubband transition energies do not match our measured layer-dependent resonances, and (2) intersubband transitions in quantum well (QW) structures are known to be forbidden unless the light field is polarized perpendicular to the QW plane.[29] BGR is primarily due to the change of electronic occupation that alters the dielectric screening and affects all electronic states simultaneously and thus could be observed in all excitonic transitions.[22,23] The detailed balance between band gap shrinkage and exciton binding energy may depend on the energy level and partly results in the reduced PB resonances in higher excitonic transitions. Although the pump photon energy is slightly lower than the probe energy in our study, this indeed reduces the contribution of Pauli blocking. We further verified that the overall transient behavior depends weakly on the pump photon energy (Figure S7), as observed in MoS_2.[23]

The PA resonances representing the excited-state electronic structures demonstrate clear layer dependence. Each transient spectrum taken at $\tau = 2$ ps was fitted with either a single or double (4L BP) Gaussian line shape to extract the resonant energy (Figure S8), and the layer-dependent PA and PB resonant energies are put together in comparison with the previous linear absorption results of the higher order subband excitonic transitions (Figure 3D).[5,6] Due to our limited probe energy window, some of the few-layer samples do not show

detectable resonances (2L and 3L), and some only have partially covered spectra (5L and 6L), leading to larger fitting errors. Nonetheless, we could see that our transient absorption results qualitatively agree with the linear absorption data and theoretical calculations,[6] reflecting the excited-state electronic structures of few-layer BP. While the PB resonance of 4L sample overlaps with the IR data, the PA resonances differ from the linear optical results with varying amounts. Such deviations indicate complex relation of the peak shifts with the layer numbers and may partly result from the uncertainty of the previous measurements and calculations.[5,6] The results of 4L BP show a peak shift of ∼100 meV, larger than that of single-layer MoS_2 measured with TA spectroscopy.[23]

Resonance-Enhanced Coherent Phonon Dynamics. As mentioned above, time-domain oscillations in PA resonant bands have been attributed to coherent phonon dynamics. CP generations have been studied in SWNTs,[24,28] multilayer graphene,[30] silicon membranes,[31] and other novel materials.[32,33] Our results reveal the exceptionally strong CP generations in few-layer BP, without resorting to the commonly used techniques, such as polarization manipulation[30] and resonant excitation.[28] In most of the few-layer BP samples we have studied (3−9L), measurable CP signals could only be detected when the probe energy is on or near PA resonances (Figure S9), while the off-resonant TA traces show a vanishing sign of CP. Such a probe resonance-enhanced CP phenomenon has never been observed in other 2D materials. To quantitatively analyze the layer-dependent CP properties, we fit the TA trances with an analytical function with a combination of carrier and CP contributions (Materials and Methods). A representative TA curve of 4L BP with fitting results is plotted in Figure 4a. It is shown that, after the femtosecond laser pulse excitation, the photoexcited carriers experience a rapid intraband relaxation (<0.3 ps, shorter than our temporal resolution) that cools the carriers down to the band edge and the band gap renormalization occurs during this process, which leads to the growth of the red-shifted PA signal. In the meantime, the impulsively heated lattice starts to vibrate, inducing the periodic TA oscillation due to strong electron−phonon coupling. The fast component of the carrier relaxation (∼5.0 ps) may originate from Auger recombination, which blueshifts the PA band as the photocarrier density decays (Figure S10). Lastly, interband recombination results in the slow relaxation of TA signal. The extracted CP components of few-layer BP (Figure 4B) show red-shifted phonon frequencies with increased layer numbers, from ∼35 cm^{-1} in 3L to ∼15 cm^{-1} in 9L BP. We attribute the CP mode to the layer-breathing mode (LBM), which generates interlayer motions perpendicular to the BP planes (B_z), as discussed in the theoretical work.[34] The volume oscillations of fewer-layer BP could modulate the strengths of optical transitions, which is reflected in the TA signals in real time. To analyze the layer-dependent CP frequencies, we applied the linear (1D) chain model to include merely the interlayer interactions between nearest neighbors:[34]

$$\omega_N = \omega_0 \sqrt{1 - \cos \frac{\pi}{N}}$$

where N represents the layer number of BP, and ω_0 is a fitting parameter. Our measured CP frequencies could be fitted by the 1D chain model with $\omega_0 = 59$ cm^{-1} (Figure 4C), which matches very well with theoretical calculation and bulk BP measurements.[34] Although our results agree qualitatively with

the low-frequency Raman results, they could not be explained by the previously assigned collective compressive mode.[12] The discrepancy might be caused by the differences in experimental methods. *N*-Layer material should in principle generate *N*-1 LBMs.[35] However, in our time-resolved measurements, only the lowest frequency CP modes were observed, in which the two halves of the stacks collectively vibrate against each other (Figure 4C, insets). The absence of other LBMs may be partly due to their weak couplings with optical transitions and partly due to our limited temporal resolution. In addition to the layer-breathing mode of few-layer BP, we also observed a strong- and long-coherence acoustic phonon mode in some of the thick BP films with an estimated thickness of 10−20 layers and ultralow CP frequency of ∼1 cm^{-1} (Figure S11). This is most likely the coherent longitudinal acoustic phonons,[36] which are difficult to detect with Raman spectroscopy and may have the potential for studying the nanomechanical properties of low-dimensional BP.

Similar to all linear and nonlinear optical anisotropies observed in bulk and thin film BP,[5,17,20] TA signals of few-layer BP also exhibit strong polarization dependence. Typical TA traces of 7L BP with both pump and probe beams polarized along AC and ZZ directions are measured on-resonance and slightly off-resonance (Figure S12). Two major features could be seen from the polarization resolved TA signals: (1) PA components from photocarriers achieve maximum intensity along the AC direction and minimum intensity along the ZZ direction; (2) CP components also demonstrate the same polarization selectivity, with a vanishing intensity along the ZZ direction. When the early time transient responses exhibit complex polarization dependences, we analyzed the polarization angle resolved TA intensity at $\tau = 16$ ps. The pronounced anisotropy of TA in few-layer BP is similar to the results of bulk and thin films,[20,27] whereas the anisotropy of CP is measured for the first time, reflecting the anisotropic electron−phonon interactions in few-layer BP.[37]

The strength of CP oscillation largely depends on the coupling between dielectric functions and lattice vibrations of materials. The quasi-covalent electronic hybridization of lone electron pairs between BP layers leads to the strong dependence of BP band structures upon interlayer distances.[34] Hence the coherent out-of-plane motion of LBM may strongly modulate the electronic transition of E_{nn}, implying that LBM is the most sensitive vibrational mode in transient optical measurements when the probe photons are in resonance with E_{nn}. In our BP data, around 20% of the total TA intensity is contributed by the LBM coherent phonons (Figure S12). Whereas for few-layer graphene and MoS_2, CP signals are too weak to be directly visualized in the pump−probe measurements without careful polarization controls.[30,38] Direct comparison between 8L BP and 2L graphene TA measurements is shown in Figure S13, indicating that the CP strength of BP is at least 1 order of magnitude larger than that of graphene. It is likely that the shear modes of BP are simultaneously excited with the LBM, but they are overwhelmed by the much stronger signals from photocarriers and LBM phonons. Although not the main focus of the current work, pump−probe measurements on thicker films could reveal important thermal and acoustic properties of layered materials[10,36,39] and will be further explored in our future studies.

Transient optical responses could be utilized to determine the layer numbers of BP with the combination of PA resonance and CP frequency, as characterized in Figures 3D and 4C. For

instance, we have analyzed the TA trace of an unknown region in a previously studied sample (Figure 1) and determined its layer number to be 7 based on its CP frequency and resonance energy. Although the TA intensity of few-layer BP is comparable to that of graphene, it does not have the simple linear relationship with the layer number as graphene does.[40] Thus, determining the layer number in few-layer BP is nontrivial with the time-domain-only measurements because of the strong probe wavelength dependence shown in this study. However, it might be realized with more advanced image processing techniques, such as the phasor and deep learning methods,[41,42] and merit further studies for rapid identification of layer numbers. With decent spatial, spectral, and temporal resolution, we could learn other fundamentally important properties of few-layer BP, including carrier diffusion, stacking order, strain, and edge effects with ultrafast microscopy.[43,44]

Conclusions. In summary, we have demonstrated that spectrally and temporally resolved pump−probe microscopy is ideal to study the ultrafast dynamics and excited-state electronic structures of few-layer BP. With this technique, layer-dependent resonances of transient absorption spectra were observed and attributed to band gap renormalization induced by strong many-body interactions of photocarriers. Our study also showed that ultrashort laser pulses could impulsively drive coherent atomic motions in BP that are strongly coupled with electronic transitions. These phenomena observed in small-area samples at room temperatures promise the potential of the few-layer BP for applications in optoelectronics, photonics, and nanomechanics, such as nanoscale modulators and photodectors.

Materials and Methods. *Sample Preparation.* Few-layer BP flakes were mechanically exfoliated on PDMS from bulk crystals (HQ Graphene, Inc.). To achieve a high optical quality, BP samples on PDMS were directly used for optical measurements without an additional sample transfer process. Another advantage for the PDMS substrate is that it is suitable for background free transmission measurements. To minimize the effect of sample degradation in air, optical measurements were typically finished within 0.5 h after sample exfoliation. The infrared transmission (extinction) spectra with photon energy from 0.46 to 1.36 eV (3750−11000 cm^{-1}) were obtained to determine the accurate layer number and the orientation of BP, using FTIR in conjunction with an infrared microscope with a 15× objective at room temperature.[6] For pump−probe measurements, the BP samples were sandwiched between a glass slide and a coverslip and then sealed with epoxy. More than 8 samples of each layer number were measured to ensure the data repeatability. All experiments were performed at room temperature under ambient conditions.

Pump−Probe Microscopy. The optical layout of our pump−probe microscope is presented in Figure S1. Briefly, a commercial femtosecond optical parametric oscillator (OPO, Insight DS+, Newport, CA) was used as the laser source, with the fundamental 1040 nm beam as the pump and the tunable output (750−990 nm) as the probe. The pump beam was modulated at 20 MHz by an electro-optical modulator (EOM), collinearly combined with the probe beam and delivered into a laser-scanning microscope (FV1200, Olympus). The laser beams were focused onto the sample with an air objective lens (UPLSAPO 20×, NA = 0.75, Olympus) to ∼1.5 μm, raster scanned by a pair of galvo mirrors, transmitted through the samples, passed through an optical filter to block the pump beam, and then directed onto a large-area silicon photodiode.

Pump fluence was kept at approximately 300 μJ/cm^2 (1.5 × 10^{15} photons/cm^2). The pump and probe beams were combined with a dichroic mirror (DMSP1000, Thorlabs) and aligned collinearly. A polarizer and half-wave plate are inserted before the microscope to control the polarization with a motorized rotational stage (K10CR1A1, Thorlabs). The probe beam was optically filtered by two low-pass filters (FF01−1010/SP-25, Semrock), collected by a photodiode, and demodulated with a commercial lock-in amplifier (HF2LI, Zurich Instruments) to extract the TA signal (ΔA). A pixel dwell time of 2 μs and image size of 320 × 320 pixels were used in the experiments. The cross-correlation between pump and probe pulses at the sample was measured to be ∼0.3 ps (Figure 1F), and the time delay interval between adjacent images was set to $\Delta \tau$ = 133 fs. A single τ scan of 20 ps costs ∼1.5 min, and a complete spectral scan costs ∼30 min.

Data Fitting. We use the analytical function to fit TA data with CP oscillations:

$$S(t) = [\delta(t) + A_1 e^{-t/\tau_1} + A_2 e^{-t/\tau_2} + A_3 e^{-t/\tau_3} \times \sin(\omega t + \varphi) + C] \otimes g(t)$$

where the δ function represents the instantaneous electronic response at time zero, the first two exponential terms represent the growth and decay of the PA signal due to carrier relaxation and BGR, the decaying sinusoid represents the CP dynamics, and the constant term roughly represents the much slower interband relaxation. $g(t)$ is a Gaussian function representing our instrument response function, which is convoluted with the above dynamical functions to represent the final signal.

■ ASSOCIATED CONTENT

ⓢ Supporting Information

The Supporting Information is available free of charge on the ACS Publications website at DOI: 10.1021/acs.nanolett.8b00551.

> Optical layouts, details of layer-dependent TA spectra and data analysis, polarization-dependent TA and CP results, and comparison between few-layer BP and graphene transient behaviors (PDF)
> Movie S1 (AVI)

■ AUTHOR INFORMATION

Corresponding Authors
*E-mail: hgyan@fudan.edu.cn.
*E-mail: minbiaoj@fudan.edu.cn.
ORCID ⊙
Guowei Zhang: 0000-0001-8905-8302
Minbiao Ji: 0000-0002-9066-4008

Author Contributions

M.J. and H.Y. conceived the experiment. G.Z. and F.W. prepared the samples and measured the infrared spectra. X.M. performed the ultrafast measurements. The manuscript was written through contributions of all authors. All authors have given approval to the final version of the manuscript. X.M. and G.Z. contributed equally.

Notes

The authors declare no competing financial interest.

■ ACKNOWLEDGMENTS

■ REFERENCES

(1) Li, L.; Yu, Y.; Ye, G. J.; Ge, Q.; Ou, X.; Wu, H.; Feng, D.; Chen, X. H.; Zhang, Y. *Nat. Nanotechnol.* **2014**, *9* (5), 372−377.

(2) Xia, F.; Wang, H.; Jia, Y. *Nat. Commun.* **2014**, *5*, 4458.

(3) Qiao, J.; Kong, X.; Hu, Z.-X.; Yang, F.; Ji, W. *Nat. Commun.* **2014**, *5*, 4475.

(4) Tran, V.; Soklaski, R.; Liang, Y.; Yang, L. *Phys. Rev. B: Condens. Matter Mater. Phys.* **2014**, *89* (23), 235319.

(5) Li, L.; Kim, J.; Jin, C.; Ye, G. J.; Qiu, D. Y.; da Jornada, F. H.; Shi, Z.; Chen, L.; Zhang, Z.; Yang, F.; et al. *Nat. Nanotechnol.* **2016**, *12* (1), 21−25.

(6) Zhang, G.; Huang, S.; Chaves, A.; Song, C.; Özçelik, V. O.; Low, T.; Yan, H. *Nat. Commun.* **2017**, *8*, 14071.

(7) Liu, H.; Neal, A. T.; Zhu, Z.; Luo, Z.; Xu, X.; Tomanek, D.; Ye, P. D. *ACS Nano* **2014**, *8* (4), 4033−4041.

(8) Wei, Q.; Peng, X. *Appl. Phys. Lett.* **2014**, *104* (25), 251915.

(9) Luo, Z.; Maassen, J.; Deng, Y.; Du, Y.; Garrelts, R. P.; Lundstrom, M. S.; Ye, P. D.; Xu, X. *Nat. Commun.* **2015**, *6*, 8572.

(10) Jang, H.; Wood, J. D.; Ryder, C. R.; Hersam, M. C.; Cahill, D. G. *Adv. Mater.* **2015**, *27* (48), 8017−22.

(11) Buscema, M.; Groenendijk, D. J.; Steele, G. A.; van der Zant, H. S.; Castellanos-Gomez, A. *Nat. Commun.* **2014**, *5*, 4651.

(12) Guo, Q.; Pospischil, A.; Bhuiyan, M.; Jiang, H.; Tian, H.; Farmer, D.; Deng, B.; Li, C.; Han, S.-J.; Wang, H. *Nano Lett.* **2016**, *16* (7), 4648−4655.

(13) Li, L.; Engel, M.; Farmer, D. B.; Han, S.-j.; Wong, H.-S. P. *ACS Nano* **2016**, *10* (4), 4672−4677.

(14) Dong, S.; Zhang, A. M.; Liu, K.; Ji, J. T.; Ye, Y. G.; Luo, X. G.; Chen, X. H.; Ma, X. L.; Jie, Y. H.; Chen, C. F.; et al. *Phys. Rev. Lett.* **2016**, *116* (8), 087401.

(15) Ling, X.; Liang, L.; Huang, S.; Puretzky, A. A.; Geohegan, D. B.; Sumpter, B. G.; Kong, J.; Meunier, V.; Dresselhaus, M. S. *Nano Lett.* **2015**, *15* (6), 4080−8.

(16) Zhang, S.; Yang, J.; Xu, R.; Wang, F.; Li, W.; Ghufran, M.; Zhang, Y.-W.; Yu, Z.; Zhang, G.; Qin, Q.; et al. *ACS Nano* **2014**, *8* (9), 9590−9596.

(17) Youngblood, N.; Peng, R.; Nemilentsau, A.; Low, T.; Li, M. *ACS Photonics* **2017**, *4* (1), 8−14.

(18) Surrente, A.; Mitioglu, A. A.; Galkowski, K.; Klopotowski, L.; Tabis, W.; Vignolle, B.; Maude, D. K.; Plochocka, P. *Phys. Rev. B: Condens. Matter Mater. Phys.* **2016**, *94* (7), 075425.

(19) Wang, K.; Szydłowska, B. M.; Wang, G.; Zhang, X.; Wang, J. J.; Magan, J. J.; Zhang, L.; Coleman, J. N.; Wang, J.; Blau, W. J. *ACS Nano* **2016**, *10* (7), 6923−6932.

(20) Ge, S.; Li, C.; Zhang, Z.; Zhang, C.; Zhang, Y.; Qiu, J.; Wang, Q.; Liu, J.; Jia, S.; Feng, J.; et al. *Nano Lett.* **2015**, *15* (7), 4650−4656.

(21) Iyer, V.; Ye, P.; Xu, X. *2D Mater.* **2017**, *4* (2), 021032.

(22) Zhu, C.; Liu, Y.; Xu, J.; Nie, Z.; Li, Y.; Xu, Y.; Zhang, R.; Wang, F. *Sci. Rep.* **2017**, *7* (1), 11221.

(23) Pogna, E. A.; Marsili, M.; De Fazio, D.; Dal Conte, S.; Manzoni, C.; Sangalli, D.; Yoon, D.; Lombardo, A.; Ferrari, A. C.; Marini, A.; et al. *ACS Nano* **2016**, *10* (1), 1182−1188.

(24) Gambetta, A.; Manzoni, C.; Menna, E.; Meneghetti, M.; Cerullo, G.; Lanzani, G.; Tretiak, S.; Piryatinski, A.; Saxena, A.; Martin, R.; et al. *Nat. Phys.* **2006**, *2* (8), 515−520.

(25) Chernikov, A.; Ruppert, C.; Hill, H. M.; Rigosi, A. F.; Heinz, T. F. *Nat. Photonics* **2015**, *9* (7), 466.

(26) Ugeda, M. M.; Bradley, A. J.; Shi, S. F.; da Jornada, F. H.; Zhang, Y.; Qiu, D. Y.; Ruan, W.; Mo, S. K.; Hussain, Z.; Shen, Z. X.; et al. *Nat. Mater.* **2014**, *13* (12), 1091−5.

(27) Suess, R. J.; Jadidi, M. M.; Murphy, T. E.; Mittendorff, M. *Appl. Phys. Lett.* **2015**, *107* (8), 081103.

(28) Korovyanko, O. J.; Sheng, C. X.; Vardeny, Z. V.; Dalton, A. B.; Baughman, R. H. *Phys. Rev. Lett.* **2004**, *92* (1), 017403.

(29) Olszakier, M.; Ehrenfreund, E.; Cohen, E.; Bajaj, J.; Sullivan, G. J. *Phys. Rev. Lett.* **1989**, *62* (25), 2997−3000.

(30) Boschetto, D.; Malard, L.; Lui, C. H.; Mak, K. F.; Li, Z.; Yan, H.; Heinz, T. F. *Nano Lett.* **2013**, *13* (10), 4620−4623.

(31) Cuffe, J.; Ristow, O.; Chávez, E.; Shchepetov, A.; Chapuis, P.-O.; Alzina, F.; Hettich, M.; Prunnila, M.; Ahopelto, J.; Dekorsy, T.; et al. *Phys. Rev. Lett.* **2013**, *110* (9), 095503.

(32) Mizoguchi, K.; Morishita, R.; Oohata, G. *Phys. Rev. Lett.* **2013**, *110* (7), 077402.

(33) Misochko, O. V.; Flock, J.; Dekorsy, T. *Phys. Rev. B: Condens. Matter Mater. Phys.* **2015**, *91* (17), 174303.

(34) Hu, Z.-X.; Kong, X.; Qiao, J.; Normand, B.; Ji, W. *Nanoscale* **2016**, *8* (5), 2740−2750.

(35) Lui, C. H.; Heinz, T. F. *Phys. Rev. B: Condens. Matter Mater. Phys.* **2013**, *87* (12), 121404.

(36) Ge, S.; Liu, X.; Qiao, X.; Wang, Q.; Xu, Z.; Qiu, J.; Tan, P. H.; Zhao, J.; Sun, D. *Sci. Rep.* **2015**, *4*, 5722.

(37) Ling, X.; Huang, S.; Hasdeo, E. H.; Liang, L.; Parkin, W. M.; Tatsumi, Y.; Nugraha, A. R.; Puretzky, A. A.; Das, P. M.; Sumpter, B. G.; et al. *Nano Lett.* **2016**, *16* (4), 2260−2267.

(38) Nie, Z. G.; Long, R.; Sun, L. F.; Huang, C. C.; Zhang, J.; Xiong, Q. H.; Hewak, D. W.; Shen, Z. X.; Prezhdo, O. V.; Loh, Z. H. *ACS Nano* **2014**, *8* (10), 10931−10940.

(39) Qin, G.; Hu, M. *Small* **2018**, *14* (12), 1702465.

(40) Miao, X.; Xuan, N.; Liu, Q.; Wu, W.; Liu, H.; Sun, Z.; Ji, M. *ACS Appl. Mater. Interfaces* **2017**, *9* (39), 34448−34455.

(41) Digman, M. A.; Caiolfa, V. R.; Zamai, M.; Gratton, E. *Biophys. J.* **2008**, *94* (2), L14−6.

(42) Fischer, M. C.; Wilson, J. W.; Robles, F. E.; Warren, W. S. *Rev. Sci. Instrum.* **2016**, *87* (3), 031101.

(43) Guo, Z.; Manser, J. S.; Wan, Y.; Kamat, P. V.; Huang, L. B. *Nat. Commun.* **2015**, *6*, 7471.

(44) Patel, H.; Havener, R. W.; Brown, L.; Liang, Y.; Yang, L.; Park, J.; Graham, M. W. *Nano Lett.* **2015**, *15* (9), 5932−7.